Measurement and simulation of the magnetic levitation characteristics of passive no-insulation coils

James G. Storey, *Member, IEEE*, Elliott Sazo, Luke Porteous, Konstantinos Bouloukakis, Mohammad Siamaki and Rodney A. Badcock *Senior Member, IEEE*

***Abstract*—The use of no-insulation coils in high-temperature superconductor levitation bearings has the potential to produce bulk-like characteristics without the associated size, quality and mechanical limitations of bulk material. Here we performed levitation force measurements on passive (open-circuit) dry-wound and solder-impregnated REBCO no-insulation coils to investigate the effect of varying turn-to-turn resistivity. Finite-element simulations employing a rotated anisotropic resistivity tensor successfully reproduced the observed behaviour, validating this approach. Low turn-to-turn resistivity facilitates the circulation of a net azimuthal current, which enhances levitation force but decays with time due to resistive dissipation. This work lays the groundwork for future research on active (powered) coils to fully realise the potential of no-insulation coils in superconducting bearings.**

***Index Terms*—Superconducting magnetic bearing, levitation force, no-insulation coils, H-formulation, anisotropic resistivity**

I. Introduction

CONTACTLESS passively stable high-temperature superconductor (HTS) levitation bearings [1]–[4] are key to unlocking a new class of rotating machines with exceptional power, efficiency reliability and lifetime, that can also operate in cryogenic and vacuum environments. Potential applications include energy storage flywheels [5]–[7], satellite reaction wheels [7], [8] and gyroscopes, turboexpanders and cryogenic liquid pumps [9]–[11].

Although the levitation phenomenon is most commonly demonstrated using solid HTS bulks, the use of coils wound from HTS tape offers advantages. Coil size scales easily with turn number, and the critical current density of commercial tapes is very high [12] with good uniformity [13]. Whereas, despite ongoing improvements in size and quality, bulk material remains brittle, prone to cracking and has a low thermal conductivity [14]. Moreover, coils can be connected to a current source allowing the levitation force to be actively tuned [15]–[17], which is beneficial for counteracting force decay phenomena [18] exhibited by bulks. Many studies of coil-based levitation bearings exist in the literature, such as [15], [19]–[22], and the fusion reactor under development at OpenStar Technologies in New Zealand is based on a large levitated HTS coil [23], [24].

Unlike insulated coils, so-called no-insulation (NI) coils [25] support current flow between turns. So far, attention has primarily focused on the self-protection afforded by this effect where currents can bypass defects or hotspots that are present in a given turn [26]. From a levitation perspective, we hypothesize that the ability of an NI coil to support non-azimuthal currents may bestow it some bulk-like characteristics in contrast to an insulated coil. Here we report an initial investigation into the effect of turn-to-turn resistivity on the levitation characteristics of passive (i.e. open-circuit) NI coils and validate the finite-element models used for understanding their physics. This work lays the groundwork for future research on active (powered) coils to fully realise the potential of no-insulation coils in superconducting bearings.

TABLE I
PARAMETERS OF THE COILS STUDIED IN THIS WORK.

Coil	1	2	3
Winding	Dry	Solder	Dry
Turns	5	6	6
ID (mm)	25	26.8	26.8
OD (mm)	26.6	28	28
d_{turn} (mm)	0.16	0.1	0.1
Height (mm)	12	12	12
$I_{c,tape}$(77 K) (A)	97	817	817

II. Experimental details

Three passive HTS no-insulation coils, summarised in Table I, are studied in this work. Coil 1 consists of five turns dry wound from older 12-mm REBCO wire tape with low critical current (I_c). The self-field tape I_c is 97 A at 77 K. Coils 2 and 3 each have six turns and are both wound from new 12-mm Fujikura FYSC-SCH12 tape [27] that has an I_c of 817 A at 77 K. Coil 2 is solder-impregnated with indium-bismuth and Coil 3 is dry wound to investigate the effect of turn-to-turn resistivity on levitation force.

The force vs displacement characteristics were measured in the test rig previously detailed in [28]. A coil is mounted inside a circular recess on the top side of an aluminium plate (see Fig. 1(a)). A matching aluminium disk is inserted into the coil bore to assist cooling. The plate is conduction-cooled by a Cryomech AL63 GM cryocooler [29]. A cylindrical N50

This work was funded by the New Zealand Ministry of Business, Innovation and Employment (MBIE) Advanced Energy technology Platform (AETP) program "High power electric motors for large scale transport" contract number RTVU2004, and the National Science Foundation IRES award #1952599. (Corresponding author: James G. Storey.)

James G. Storey and Luke Porteous are with the Robinson Research Institute, Victoria University of Wellington, Lower Hutt 5046, New Zealand (e-mail: james.storey@vuw.ac.nz). Elliott Sazo is with the Department of Physics, California State University, San Bernadino, California, U.S.A. Konstantinos Bouloukakis and Mohammad Siamaki are with with OpenStar Technologies, Wellington 6035, New Zealand and and Rodney A. Badcock is with OpenStar Technologies, Wellington 6035, New Zealand as well as Robinson Research Institute, Victoria University of Wellington, and Dodd-Walls Centre for Photonics and Quantum Technologies, Lower Hutt 5046, New Zealand

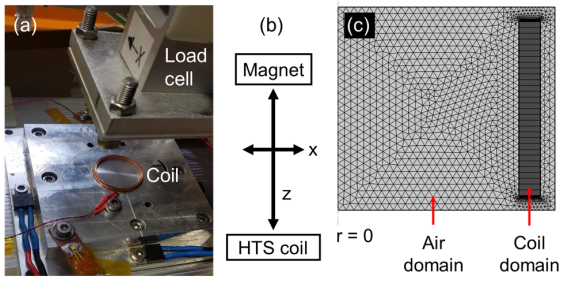

Fig. 1. (a) Photograph of a 5-turn dry-wound coil installed inside the force-displacement measurement rig. A permanent magnet is mounted to the underside of the load cell. (b) Movement axes of the magnet. (c) 2D axisymmetric mesh used in the H-formulation finite-element model.

NdFeB permanent magnet (20 mm diameter, 10 mm height, B_r = 1.4 T) is mounted to a three-axis load cell and the forces on the magnet are recorded as it moves above the coil. Movement is possible in the vertical z-axis and a single lateral x-axis (Fig. 1(b)). The positions are measured by two linear variable differential transformer sensors. The following experiments are performed: i) Zero-field-cooled (ZFC) vertical. The coil is cooled into the superconducting state with the magnet at z = 50 mm above the coil. The magnet is then moved down to z = 2 mm and back up to 50 mm at a constant speed. ii) Force decay. The coil is cooled into the superconducting state with the magnet at z = 50 mm. The magnet is moved down to z = 2 mm and is held there for several minutes. iii) Field-cooled (FC) vertical. The magnet is set at z = 7 mm before the coil is cooled into the superconducting state. The magnet is cycled vertically in the sequence z = [7, 2, 12, 2, 7] mm at a constant speed. iv) Field-cooled lateral. The magnet is set at z = 2 mm before the coil is cooled into the superconducting state. The magnet is cycled laterally in the sequence x = [0, x_m, $-x_m$, x_m, 0] mm at a constant speed, where x_m is 1 or 5 mm.

III. Simulation Details

To simulate the levitation forces, the 2D axisymmetric segregated H-formulation approach for bulk bearings from ref. [30] was adapted by incorporating the rotated anisotropic resistivity model for no-insulation coils from ref. [31]. This involves replacing the scalar expression for the non-linear resistivity with a tensor given by

$$\boldsymbol{\rho}_{\text{coil}} = \begin{bmatrix} \rho_{rr} & \rho_{r\phi} & 0 \\ \rho_{\phi r} & \rho_{\phi\phi} & 0 \\ 0 & 0 & \rho_z \end{bmatrix}_{\hat{r},\hat{\phi},\hat{z}} \tag{1}$$

with components

$$\rho_{rr} = \rho_n \cos^2\alpha + \rho_{sc} \sin^2\alpha \tag{2}$$

$$\rho_{r\phi} = \rho_{\phi r} = \tfrac{1}{2}(-\rho_n + \rho_{sc}) \sin(2\alpha) \tag{3}$$

$$\rho_{\phi\phi} = \rho_{sc} \cos^2\alpha + \rho_n \sin^2\alpha \tag{4}$$

$$\rho_z = \rho_{sc} \tag{5}$$

α is the difference in angle between the spiral and cylindrical coordinate systems

$$\alpha = \pm \arctan\left(\frac{d}{2\pi r}\right) \tag{6}$$

and ρ_n is the turn-to-turn resistivity

$$\rho_n = \frac{R_{\text{ct}}}{d} \tag{7}$$

where R_{ct} is the specific contact resistivity and d is the turn thickness.

The non-linear resistivity of the superconductor is given by the E-J power law

$$\rho_{sc} = \frac{E_c}{J_c} \left| \frac{\mathbf{J}_{\parallel}}{J_c} \right|^{n-1} \tag{8}$$

where $E_c = 1$ μV/cm and $n = 30$. For simplicity we assume a constant (field-independent) critical current density (J_c). The in-plane current density of the superconducting tape is $|\mathbf{J}_{\parallel}| = \sqrt{J_T^2 + J_z^2}$ where $J_T = J_r \sin(\alpha) + J_\phi \cos(\alpha)$.

The H-formulation simulations were performed in COMSOL Multiphysics [32] using the Magnetic Field Formulation (mfh) interface with the MUMPS direct solver. An example of the meshed air and coil domains is shown in Fig. 1(c). Relative and absolute tolerances were set to 10^{-5} and 10^{-4} respectively. Note that it is essential to use quadratic discretization to obtain converging mesh-independent results. As usual, the sum of the external field from the permanent magnet (stored in a look-up table) and self-field produced from the coil was applied as a boundary condition on the air domain [30]. Once the physical dimensions of the coil and magnet are set, J_c and R_{ct} are the only adjustable parameters for matching simulations to the data.

IV. Results

A. Coil 1: Five-Turn Dry-Wound

Coil 1, the low-I_c five-turn dry-wound coil, was measured at 27, 55 and 77 K. The ZFC, FC and lateral force-displacement data are shown in Figs. 2(a) – (c). The magnet speed was 1 mm/s. Simulated ZFC and FC curves are overlaid. J_c and R_{ct} values were selected by fitting to the FC data and then the ZFC curves were calculated with those same values. In both cases, the shape of the loops is closely reproduced. The physics is determined by J_c. Hysteresis in the levitation force is due to irreversibility in the penetration of induced currents [33], with lower J_c leading to larger penetration and therefore larger hysteresis. Here the loops exhibit large hysteresis, indicative of a low J_c. At 77 K, J_c = 23 MA/m^2. This corresponds to a coil I_c = 44 A, which is suppressed compared to the measured self-field tape I_c of 97 A. Likely causes include the field from the permanent magnet, the self-field of the coil, and winding stress in the tape. The magnitude of the forces, given by the integral of $J \times B$ [30], decreases with temperature due to the concomitant decrease in J_c [28], [34], [35].

The value of R_{ct} = 10 $\mu\Omega$cm^2 is independent of temperature and can be considered a lower limit. That is, increasing R_{ct} further has little effect on the results, indicating that the coil turns are effectively insulated from each other. This was supported by subsequent measurements which showed no change in force after insulating between turns with a layer of Kapton. The lateral restoring force and stiffness (given by the slope) decreases with temperature. Simulating lateral forces requires a 3D model and is part of ongoing work.

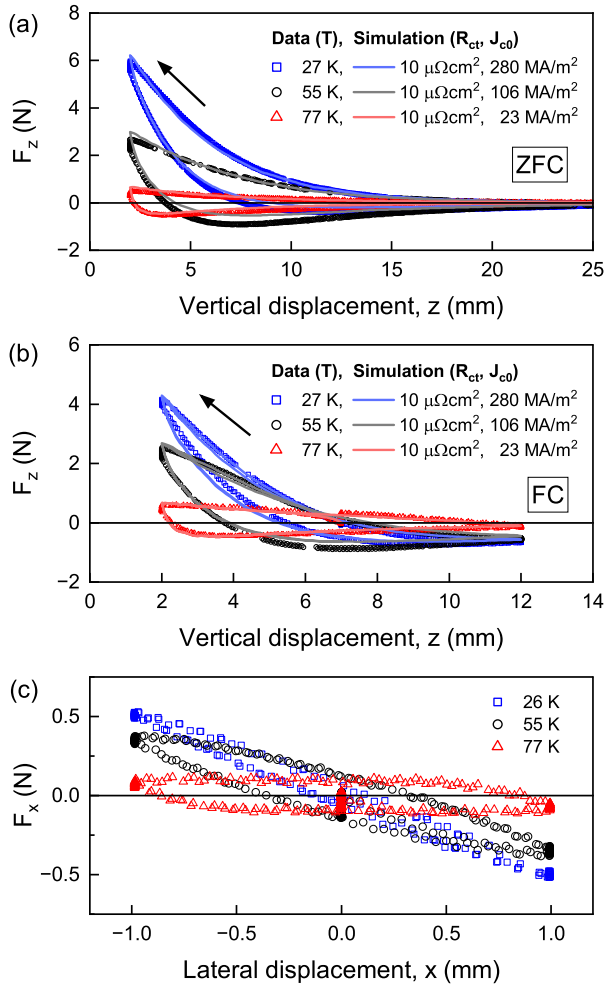

Fig. 2. Force vs displacement curves for the 5-turn 25 mm inner diameter dry-wound coil at 27, 55 and 77 K. The magnet speed was 1 mm/s. (a) Zero-field-cooled and (b) field-cooled levitation force measurements (symbols) and simulations (lines). Arrows indicate the magnet descending towards the coil. (c) Measured restoring force as a function of lateral displacement.

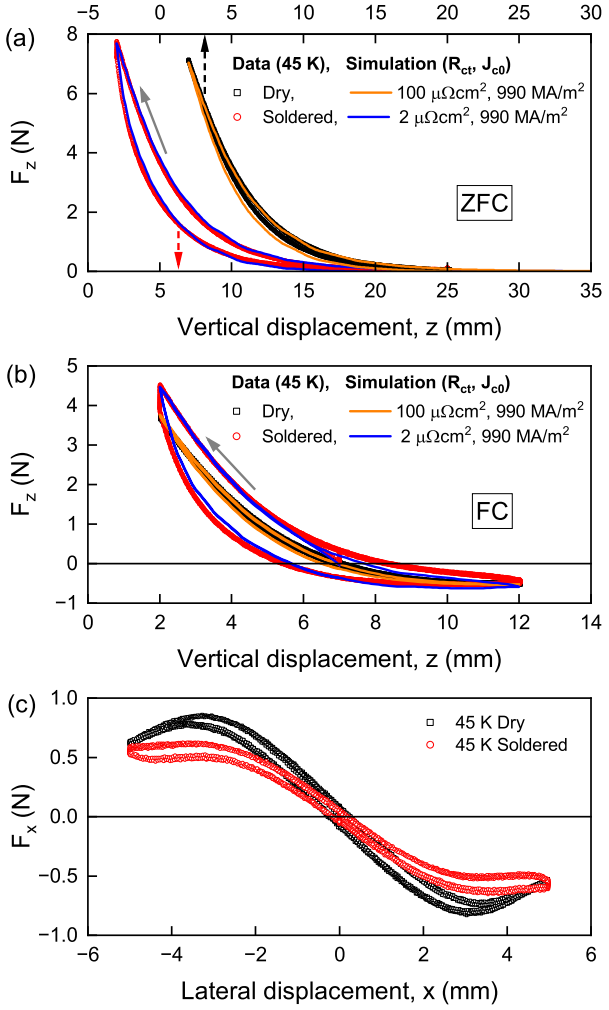

Fig. 3. Force vs displacement curves for 6-turn 28 mm outer diameter dry-wound and solder-impregnated coils at 45 K. The magnet speed was 0.5 mm/s. (a) Zero-field-cooled and (b) field-cooled levitation force measurements (symbols) and simulations (lines). The dry-wound plot in (a) has been shifted to the right for clarity. Solid arrows indicate the magnet descending towards the coil. (c) Measured restoring force as a function of lateral displacement.

B. Coils 2 & 3: Solder-Impregnated vs Dry-Wound

ZFC, FC and lateral force-displacement measurements performed at 45 K on solder-impregnated (Coil 2) and dry-wound (Coil 3) coils are shown in Figs. 3(a) – (c). The magnet speed was 0.5 mm/s. Both coils consist of 6 turns of high-I_c tape from the same batch. The ZFC and FC loops for the dry-wound coil have very small hysteresis, indicating a high J_c. In contrast, measurements on the solder-impregnated coils exhibit a larger hysteresis. The solder-impregnated coil also produces slightly higher maximum forces at $z = 2$ mm. Simulated curves (overlaid) reproduce the features seen in the data. J_c is the same for both coils, showing that it has not been affected by the solder-impregnation process. Calculations for the two coils differ only in the value assumed for the $R_{\rm ct}$. The dry-wound value (100 $\mu\Omega$cm^2) implies that the turns are effectively insulated, whereas the low value for the solder-impregnated coil implies that turn-to-turn currents play a role in causing the larger hysteresis. In contrast, the lateral forces have similar levels of hysteresis.

Measurements and simulations of the levitation force decay with time at 45 K are shown in Fig. 4. They show that the higher levitation force achieved by the solder-impregnated coil is only temporary, with the force decaying towards dry-wound values with time. The maximum force also depends on the magnet approach speed. In contrast, no speed dependence is found in measurements or simulations of the dry-wound coil suggesting that this effect is due to turn-to-turn currents.

To test this hypothesis, a 3D H-formulation model of a bilayer HTS-metal coil was constructed using the parametric equations for an Archimedean spiral

$$x = (r + sd)\cos(2\pi s) \tag{9}$$

$$y = (r + sd)\sin(2\pi s) \tag{10}$$

where r is the inner radius, d is the turn-to-turn distance, and the parameter s ranges from zero to the number of turns. The finite-element mesh is shown in Fig. 5. The resistivity for the HTS layer was $\rho_{sc} = (E_c/J_c)|\mathbf{J}/J_c|^{n-1}$ with $J_c = 2.4 \times 10^9$ A/m^2 and $n = 21$, and the metal layer was set to copper ($1.77 \times 10^{-8}\Omega$m). The same magnet as above was assumed.

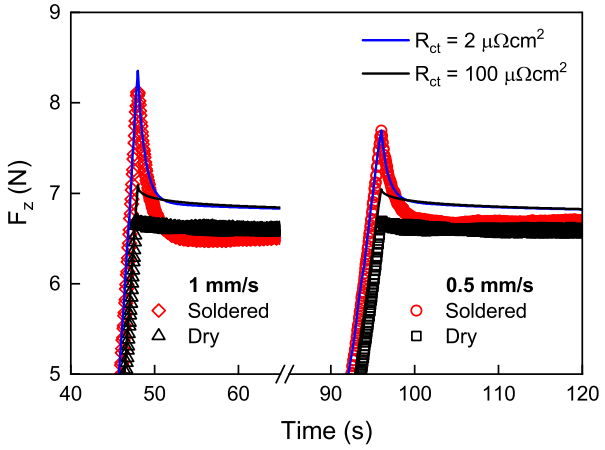

Fig. 4. (Symbols) Time decay of the levitation force from the dry and solder-impregnated coils at 45 K after the magnet was moved from z = 50 to 2 mm at speeds of 1 mm/s and 0.5 mm/s. (Lines) Simulated force decay with $R_{ct} = 2$ and 100 $\mu\Omega$cm^2.

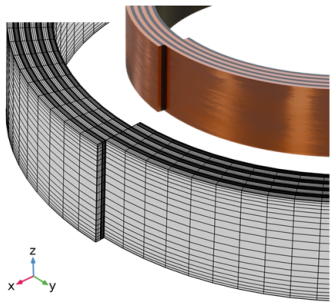

Fig. 5. Four-turn bilayer HTS-metal 3D spiral model (air domain not shown). The HTS layer has the higher density mesh. Inner radius r = 12 mm, bilayer thickness d = 0.25 + 0.25 mm, height 5 mm, $J_c = 2.4 \times 10^9$ A/m^2, n = 21.

To greatly reduce memory usage and simulation time, the self-field correction to the applied magnetic field was neglected. Doing so leads to a slight underestimation of force magnitude but it is the qualitative behaviour, especially of the current distribution in the two layers, that is the focus here.

Figure 6(a) presents the simulated force decay curve for the bilayer HTS-metal coil, alongside cases where the metal layer is replaced by air or a second HTS layer. The bilayer coil reproduces the phenomenology observed in Fig. 4, where a larger peak force is reached which subsequently decays towards the insulated coil case.

With this model, the current distribution in the different layers can be observed. Components of the current density tangential (J_T) and normal (J_n) to the coil winding in the YZ-plane were calculated using the equations derived in ref. [36]. Figure 6(c) shows that J_n in the metal layers decays after the magnet stops moving at 48 seconds. Integrating J_T in the HTS layers gives the net azimuthal current around the coil, shown in Fig. 6(b). Looking first at the the HTS + air case, the induced current flows in one direction along the top half of the tape before reversing direction at the end of the tape and returning along the bottom half, resulting in no net azimuthal current [20]. The HTS + HTS case is essentially a bulk superconducting ring, where a net azimuthal persistent

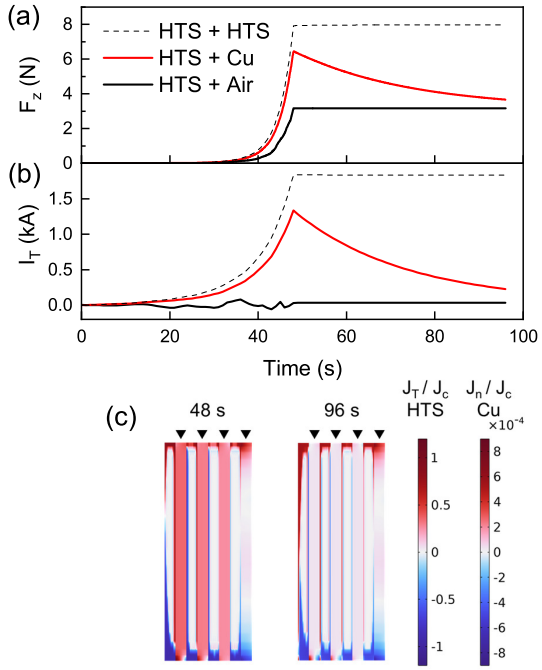

Fig. 6. (a) Simulated force decay curve from the bilayer HTS-metal 3D spiral model (red line). Shown for comparison are cases where the metal layer has been replaced by air (black line) and HTS (dashed line). (b) Net current tangential to the winding in the HTS layers. (c) J_T in the HTS layers, and J_n in the metal layers (denoted by triangles) at 48 and 96 seconds.

current is induced. HTS + Cu is an intermediate case where turn-to-turn currents through the copper layer facilitate a net azimuthal current. However the finite turn-to-turn resistivity causes the net azimuthal current, and therefore the levitation force, to decay with time. This is most noticeable after the magnet has stopped moving.

V. Conclusions

In this work the levitation and restoring forces of passive dry-wound and solder-impregnated HTS coils were measured. The data was successfully modeled with a homogenised 2D axisymmetric H-formulation model employing a rotated anisotropic resistivity. A 3D bilayer spiral model was used to further understand the physics. Compared to superconducting bulks, the levitation force produced by passive no-insulation coils with low turn-to-turn resistivity has a large time dependence. This arises from the finite turn-to-turn resistance which causes net azimuthal induced current, beneficial for levitation, to decay with time. A consequence is that the cyclic vertical force-displacement characteristics, namely the maximum force and hysteresis, depend on the speed of the moving magnet. In the quasi-static regime, the levitation forces are the same as passive insulated coils which have zero net azimuthal current. Avenues for future work include testing the validity of the modelling approach on coils of different size and shape, as well as exploring the difference between actively powered dry-wound and no-insulation coils for use as tunable bearings.

REFERENCES

[1] J. R. Hull, "Superconducting bearings," *Superconductor Science and Technology*, vol. 13, no. 2, p. R1, Feb. 2000, doi:10.1088/0953-2048/13/2/201.

[2] K. B. Ma, Y. V. Postrekhin, and W. K. Chu, "Superconductor and magnet levitation devices," *Review of Scientific Instruments*, vol. 74, no. 12, pp. 4989–5017, Dec. 2003, doi:10.1063/1.1622973.

[3] T. S. Slininger, W. Chan, E. L. Severson, and B. Jawdat, "An overview on passive magnetic bearings," in *2021 IEEE International Electric Machines & Drives Conference (IEMDC)*, 2021, pp. 1–8, Art. no. 3800215, doi:10.1109/IEMDC47953.2021.9449571.

[4] D. K. Supreeth, S. I. Bekinal, S. R. Chandranna, and M. Doddamani, "A review of superconducting magnetic bearings and their application," *IEEE Transactions on Applied Superconductivity*, vol. 32, no. 3, pp. 1–15, 2022, Art. no. 3800215, doi:10.1109/TASC.2022.3156813.

[5] M. Strasik, J. R. Hull, J. A. Mittleider, J. F. Gonder, P. E. Johnson, K. E. McCrary, and C. R. McIver, "An overview of Boeing flywheel energy storage systems with high-temperature superconducting bearings," *Superconductor Science and Technology*, vol. 23, no. 3, p. 034021, Feb. 2010, doi:10.1088/0953-2048/23/3/034021.

[6] F. N. Werfel, U. Floegel-Delor, R. Rothfeld, T. Riedel, B. Goebel, D. Wippich, and P. Schirrmeister, "Superconductor bearings, flywheels and transportation," *Superconductor Science and Technology*, vol. 25, no. 1, p. 014007, Dec. 2011, doi:10.1088/0953-2048/25/1/014007.

[7] J. Tang, J. Fang, and S. S. Ge, "Roles of superconducting magnetic bearings and active magnetic bearings in attitude control and energy storage flywheel," *Physica C: Superconductivity*, vol. 483, pp. 178–185, 2012, doi:10.1016/j.physc.2012.07.007.

[8] K. Ma, Y. Zhang, Y. Postrekhin, and W.-K. Chu, "HTS bearings for space applications: reaction wheel with low power consumption for mini-satellites," *IEEE Transactions on Applied Superconductivity*, vol. 13, no. 2, pp. 2275–2278, 2003, doi:10.1109/TASC.2003.813064.

[9] R. Decher, P. Peters, R. Sisk, E. Urban, M. Vlasse, and D. Rao, "High temperature superconducting bearing for rocket engine turbopumps," *Applied Superconductivity*, vol. 1, no. 7, pp. 1265–1278, 1993, doi:10.1016/0964-1807(93)90435-5.

[10] J. Xu, C. Li, X. Miao, C. Zhang, and X. Yuan, "An overview of bearing candidates for the next generation of reusable liquid rocket turbopumps," *Chinese Journal of Mechanical Engineering (English Edition)*, vol. 33, no. 1, p. 26, 2020, doi:10.1109/10.1186/s10033-020-00442-6.

[11] L. Ai, G. Zhang, X. Xu, H. Feng, and W. Cao, "Analysis and testing of a superconducting maglev submersible cryogenic liquid pump," *IET Electric Power Applications*, vol. 16, no. 4, pp. 498–510, 2022, doi:10.1049/elp2.12171.

[12] S. C. Wimbush and N. M. Strickland, "A public database of high-temperature superconductor critical current data," *IEEE Transactions on Applied Superconductivity*, vol. 27, no. 4, pp. 1–5, 2017, Art. no. 8000105, doi:10.1109/TASC.2016.2628700.

[13] A. Molodyk, S. Samoilenkov, A. Markelov, P. Degtyarenko, S. Lee, V. Petrykin, M. Gaifullin, A. Mankevich, A. Vavilov, B. Sorbom, J. Cheng, S. Garberg, L. Kesler, Z. Hartwig, S. Gavrilkin, A. Tsvetkov, T. Okada, S. Awaji, D. Abraimov, A. Francis, G. Bradford, D. Larbalestier, C. Senatore, M. Bonura, A. Pantoja, S. Wimbush, N. Strickland, and A. Vasiliev, "Development and large volume production of extremely high current density $YBa_2Cu_3O_7$ superconducting wires for fusion," *Scientific Reports*, vol. 11, no. 1, p. 2084, 2021, doi:10.1038/s41598-021-81559-z.

[14] D. K. Namburi and D. A. Cardwell, *Design of Cuprate HTS Superconductors*. Singapore: Springer Nature Singapore, 2022, pp. 239–270, doi:10.1007/978-981-19-1211-5_9.

[15] F. Sass, G. G. Sotelo, A. Polasek, and R. de Andrade, "Application of 2G-tape for passive and controlled superconducting levitation," *IEEE Transactions on Applied Superconductivity*, vol. 21, no. 3, pp. 1511–1514, 2011, doi:10.1109/TASC.2010.2103539.

[16] T. Espenhahn and R. Hühne, "A fully superconducting magnetic bearing with a jointless coil excited by a superconducting dynamo," *Superconductor Science and Technology*, vol. 37, no. 9, p. 095021, Aug. 2024, doi:10.1088/1361-6668/ad6d9d.

[17] Q. Xu, Y. Lin, Y. Tan, and J. Geng, "Tunable superconducting magnetic levitation with self-stability," *arXiv:2403.19168*, 2024, doi:10.48550/arXiv.2403.19168.

[18] H. Liao, J. Zheng, L. Jin, H. Huang, Z. Deng, Y. Shi, D. Zhou, and D. A. Cardwell, "Dynamic levitation performance of Gd-Ba-Cu-O and Y-Ba-Cu-O bulk superconductors under a varying external magnetic field," *Superconductor Science and Technology*, vol. 31, no. 3, p. 035010, Feb. 2018, doi:10.1088/1361-6668/aaa82a.

[19] A. Patel, S. C. Hopkins, A. Baskys, V. Kalitka, A. Molodyk, and B. A. Glowacki, "Magnetic levitation using high temperature superconducting pancake coils as composite bulk cylinders," *Superconductor Science and Technology*, vol. 28, no. 11, p. 115007, Sep. 2015, doi:10.1088/0953-2048/28/11/115007.

[20] E. Kurbatova, P. Kurbatov, E. Kuschenko, and Y. Kulaev, "Using of HTS tape coils for the design of a magnetic bearing," *Journal of Physics: Conference Series*, vol. 1559, no. 1, p. 012121, Jun. 2020, doi:10.1088/1742-6596/1559/1/012121.

[21] W. Li, T. Yang, and Y. Xin, "Principle, modeling and experiment of a new axial-type superconducting magnetic bearing with superconducting coil," *IEEE Transactions on Applied Superconductivity*, vol. 34, no. 5, pp. 1–5, 2024, Art. no. 3601705, doi:10.1109/TASC.2024.3374258.

[22] F. G. R. Martins, G. d. Santos, B. M. O. Santos, F. Sass, E. Rodriguez, G. G. Sotelo, and R. de Andrade, "Vertical and horizontal force measurements of a double crossed loop," *IEEE Transactions on Applied Superconductivity*, vol. 34, no. 3, pp. 1–5, 2024, Art. no. 3601305, doi:10.1109/TASC.2024.3360938.

[23] M. Harris. (2024) A new fusion prototype floats into action. IEEE Spectrum. Accessed Aug. 26, 2025. [Online]. Available: https://spectrum.ieee.org/dipole-fusion-reactor

[24] C. Chisholm, T. Berry, D. Garnier, R. Badcock, G. Bioletti, K. Bouloukakis, E. Brewerton, M. Buchanan, P. Burt, E. Chambers, K. Chappell, P. Coulson, R. Davidson, J. Ellingham, P. Geursen, K. Hamilton, R. Hu, E. Hunter, J. Jones, P. Kusay, Z. Lazić, B. Leuw, M. Lynch, R. Mataira, M. McCrohon, L. Meadows, J. Morris, R. Nowacki, J. Purvis, J. Rice, M. Rutten, S. Schimanski, A. Sharma, M. Siamaki, A. Simpson, T. Simpson, B. Smith, E. Stiers, E. Swanson-Dobbs, J. Todd, E. Treacher, J. Tyler, S. Venuturumilli, H. Weijers, T. Wordsworth, and N. Zhou, "Design and initial results from the "Junior" levitated dipole experiment," *Fusion Engineering and Design*, vol. 223, p. 115551, 2026, doi:10.1016/j.fusengdes.2025.115551.

[25] S. Hahn, D. K. Park, J. Bascunan, and Y. Iwasa, "HTS pancake coils without turn-to-turn insulation," *IEEE Transactions on Applied Superconductivity*, vol. 21, no. 3, pp. 1592–1595, 2011, doi:10.1109/TASC.2010.2093492.

[26] S. Hahn, K. Radcliff, K. Kim, S. Kim, X. Hu, K. Kim, D. V. Abraimov, and J. Jaroszynski, "'Defect-irrelevant' behavior of a no-insulation pancake coil wound with REBCO tapes containing multiple defects," *Superconductor Science and Technology*, vol. 29, no. 10, p. 105017, Sep. 2016, doi:10.1088/0953-2048/29/10/105017.

[27] Superconductors - Fujikura. Accessed Sept. 10, 2025. [Online]. Available: https://www.europe.fujikura.com/markets/industrial/superconductors

[28] J. G. Storey, M. Szmigiel, F. Robinson, S. C. Wimbush, and R. A. Badcock, "Stiffness enhancement of a superconducting magnetic bearing using shaped YBCO bulks," *IEEE Transactions on Applied Superconductivity*, vol. 30, no. 4, pp. 1–6, 2020, Art. no. 600706, doi:10.1109/TASC.2020.2982884.

[29] Oxford Cryosystems Gifford McMahon Cryocoolers. Accessed Feb. 3, 2026. [Online]. Available: https://bluefors.com/products/gifford-mcmahon-cryocoolers/al63/

[30] L. Quéval, K. Liu, W. Yang, V. M. R. Zermeõ, and G. Ma, "Superconducting magnetic bearings simulation using an H-formulation finite element model," *Superconductor Science and Technology*, vol. 31, no. 8, p. 084001, Jun. 2018, doi:10.1088/1361-6668/aac55d.

[31] R. C. Mataira, M. D. Ainslie, R. A. Badcock, and C. W. Bumby, "Finite-element modelling of no-insulation HTS coils using rotated anisotropic resistivity," *Superconductor Science and Technology*, vol. 33, no. 8, p. 08LT01, Jun. 2020, doi:10.1088/1361-6668/ab9688.

[32] COMSOL Multiphysics® v. 6.3. http://www.comsol.com. COMSOL AB, Stockholm, Sweden. Accessed Aug. 18, 2025.

[33] C. Navau, N. Del-Valle, and A. Sanchez, "Macroscopic modeling of magnetization and levitation of hard type-II superconductors: The critical-state model," *IEEE Transactions on Applied Superconductivity*, vol. 23, no. 1, pp. 8 201 023–8 201 023, 2013, Art. no. 8201023, doi:10.1109/TASC.2012.2232916.

[34] C. Chiang, C. Yang, P. Hsieh, and W. Chan, "Levitation force measurement at different temperatures for YBCO superconductor," *Journal of Low Temperature Physics*, vol. 131, no. 3-4, pp. 743–746, 2003, doi:10.1023/A:1022925419581.

[35] J. Zhou, X.-Y. Zhang, and Y.-H. Zhou, "Temperature dependence of levitation force and its relaxation in a HTS levitation system," *Physica C: Superconductivity*, vol. 470, no. 5, pp. 336–339, 2010, doi:10.1016/j.physc.2009.12.070.

[36] Z. Zhong, W. Wu, G. Ma, and Z. Jin, "Study of the demagnetization behavior of no-insulation persistent-current mode HTS coils under

external AC fields by 3D FEM simulation," *Superconductor Science and Technology*, vol. 37, no. 4, p. 045011, Mar. 2024, doi:10.1088/1361-6668/ad2300.